

The Quasi-Stationary Structure of Radiating Shock Waves.

II. The Two-Temperature Fluid

M W Sincell

Dpartement d'Astrophysique Extragalactique et de Cosmologie
Observatoire de Paris-Meudon

M Gehmeyr, D Mihalas

Department of Astronomy, University of Illinois at Urbana-Champaign
Laboratory for Computational Astrophysics, National Center for Supercomputing Applications

ABSTRACT

We solve the equations of radiation hydrodynamics in the two-temperature fluid approximation on an adaptive grid. The temperature structure depends upon the electron-ion energy exchange length, l_{ei} , and the electron conduction length, l_{ec} . Three types of radiating shock structure are observed: subcritical, where preheating of the unshocked gas is negligible; electron supercritical, where radiation preheating raises the temperature of the unshocked electron fluid to be equal to the final electron temperature; supercritical, where preheating and electron-ion energy exchange raise the preshock $T_{e,i}$ to their final post shock values. No supercritical shock develops when l_{ei} is larger than the photospheric depth of the shocked gas because a negligible amount of the ion energy is transferred to the electrons and the shock is weakly radiating. Electron conduction smooths the T_e profile on a length scale l_{ec} , reducing the radiation flux.

Keywords: Radiating shock waves – Numerical methods

Correspondence to: M. W. Sincell, Mark.Sincell@daec.obspm.fr

1. Introduction

The structure and dynamics of radiative shock waves are difficult to model because processes in the shock front occur on length scales that are many orders of magnitude smaller than the typical length scales for other gradients in the fluid variables (*e.g.*, the velocity field in an accretion flow). There are two standard methods for computing the structure of shocked fluids. The first is to treat the shock as a discontinuity and invoke conservation laws to relate physical quantities on either side of the shock. Analytic models of shock waves in plasmas have been constructed using this approach (Zel'dovich and Raizer 1967, Shafranov 1967) but these solutions require many

simplifying assumptions which limit the applicability of the results. The second method, common in numerical solutions, is to introduce an expression for an artificial viscosity to spread the shock over a few grid points. The magnitude of the artificial viscosity is usually chosen to be many orders of magnitude larger than the physical viscosity because the Courant limit imposes strong constraints on the maximum time step (Klein, *et al.* 1983, Burger and Katz 1983).

Formulating the numerical problem on an adaptive grid can dramatically increase the effective resolution of the grid and reduce the spurious effects of artificial viscosity. Dorfi and Drury (1987) solved the one-dimensional hydrodynamic equations on an adaptive grid. They adopted a simple grid equation which distributes grid points uniformly along the arc length of a graph of the solution variables and solved two standard problems: the shock tube and a spherical blast wave. In both cases, the adaptive grid concentrated many grid points at discontinuities in the flow. Although artificial viscosity is still needed to spread the discontinuity over a few grid points, the physical separation of each point is small compared to the length scale of the gradients in the physical quantities and the shock front appears infinitely steep. Gehmeyr and Mihalas (1994) demonstrated that this same equation can be used to resolve discontinuities in radiating flows and they performed a preliminary numerical study of radiating shock waves. A detailed study of the structure of a radiating shock wave for a single temperature fluid was carried out in Sincell, *et al.* (1997). In this paper, we extend the work of Sincell, *et al.* (1997) to a fully ionized plasma.

The gas upstream of the shock is assumed to be cold and at rest. However, we assume that the gas is always fully ionized. A supersonic piston (speed u_p) drives a collisional shock wave into the cold gas and the wave propagates into the unshocked material at a speed $D > u_p$. The structure of the shock front is steady when viewed in a reference frame moving with the front and, in this frame, the upstream gas flows into the shock at the shock speed D . The shocked gas moves away from the discontinuity at a velocity $D - u_p$.

The kinetic energy of the inflowing gas is converted into thermal energy of the ions. The ratio of the kinetic energy transferred to the ions to that transferred to electrons is $\sim m_i/m_e$, where $m_{i,e}$ are the masses of the ions and electrons, respectively. As a consequence, the increase in the electron temperature caused by viscous heating at the shock front is negligible. The dominant source of electron heating at the shock front is adiabatic compression. The plasma remains neutral and so the electron number density must change in strict proportion with the ion density. This results in compressional heating of the electrons as the gas passes through the discontinuity. For a gas with an adiabatic index of 5/3, this increases the electron temperature by at most a factor of 2.5 (Zeldovich and Raizer 1967).

The ratio of the electron and ion temperatures outside of the shock front is determined by two length scales. The ion temperature exceeds the electron temperature to a distance $l_{ei} \sim \tau_{ei}D$ behind the shock, where τ_{ei} is the time scale for energy exchange between the electron and ion fluids. Electron conduction transports energy over a distance $l_{ec} \sim \kappa_{ec}/D$, where κ_{ec} is the electron conduction coefficient. Conduction can raise the preshock electron temperature above the ion

temperature.

The electron gas upstream from the shock is also heated by radiation from the shocked gas. If the shock is strong enough, the temperature of the preheated electron fluid rises to be equal to the temperature of the shocked gas. At this strength the shock is called supercritical. A full discussion of sub- and supercritical shock waves is found in Sincell, *et al.* (1997).

We compute the structure of a radiating shock wave in a fully ionized gas for a simple model problem: a piston moving supersonically through a spherical shell of cold gas at initially constant density. We also assume that the electron-ion energy exchange rate is directly proportional to the difference in the electron and ion temperatures and the electron conduction flux is proportional to the electron temperature gradient. The proportionality coefficients are all taken as constants. Although this model is too simplified to treat realistic problems, it demonstrates the power of the adaptive grid when applied to two-temperature flows and illustrates the effects of conduction and electron-ion energy exchange on the structure of the shock wave.

The equation set and methodology are discussed in chapter 2. and the results for a series of models are presented in chapter 3. We conclude in chapter 4.

2. Equations and Methodology

We use the TITAN code (Gehmeyr and Mihalas 1994, Sincell, *et al.* 1997) to solve the time-dependent equations of radiation hydrodynamics on an adaptive grid. Gehmeyr and Mihalas (1994) provide a detailed description of TITAN so we will only summarize the key features of the code here. The equations of radiation hydrodynamics in the two fluid approximation (electron and ions are treated as separate fluids) are the continuity equation

$$D_t(\rho) + \rho \frac{\partial(r^2 u)}{r^2 \partial r} = 0, \quad (1)$$

the gas momentum equation

$$\rho D_t(u) + \frac{\partial P_e}{\partial r} + \frac{\partial(r^3 P_Q)}{r \partial r} - \frac{\rho \kappa}{c} F_r = 0, \quad (2)$$

the radiation momentum equation

$$\rho D_t\left(\frac{F_r}{\rho c^2}\right) + \frac{\partial P_r}{\partial r} + \frac{3P_r - E_r}{r} + \frac{F_r}{c^2} \frac{\partial u}{\partial r} + \frac{\rho \kappa}{c} F_r = 0, \quad (3)$$

the radiation energy equation

$$\rho D_t\left(\frac{E_r}{\rho}\right) + \frac{\partial(r^2 F_r)}{r^2 \partial r} + P_r \frac{\partial(r^2 u)}{r^2 \partial r} + (E_r - 3P_r) \frac{u}{r} + \rho \kappa c (E_r - a_r T_e^4) = 0, \quad (4)$$

the ion energy equation

$$\rho D_t(e_i) + P_i \frac{\partial(r^2 u)}{r^2 \partial r} + P_Q \left[\frac{\partial u}{\partial r} - \frac{u}{r} \right] + \Lambda_{ei} \frac{k_B}{(\gamma - 1)m_p} (T_i - T_e) = 0; \quad (5)$$

and the total energy equation

$$\begin{aligned} \rho D_t(e_e + e_i + \frac{E_r}{\rho}) + \frac{\partial(r^2 F_r)}{r^2 \partial r} + (P_e + P_i + P_r) \frac{\partial(r^2 u)}{r^2 \partial r} + P_Q \left[\frac{\partial u}{\partial r} - \frac{u}{r} \right] \\ + (E_r - 3P_r) \frac{u}{r} + \frac{\partial}{\partial r} \left(\rho \kappa_{ec} r^2 \frac{\partial T_e}{\partial r} \right) = 0, \end{aligned} \quad (6)$$

where $D_t(x) = \partial x / \partial t + u \partial x / \partial r$ is the Lagrangean time derivative operator. We assume a perfect gas equation of state with an adiabatic index of $\gamma = 5/3$, a constant absorptive opacity (κ), electron conduction coefficient (κ_{ec}) and the electron-ion energy exchange coefficient (Λ_{ei}). The radiation pressure (P_r) and energy density (E_r) are related by a variable Eddington factor, $f_E = P_r / E_r$. The Eddington factors are computed with a formal integration of the time-independent radiative transfer equation (*e.g.*, Mihalas and Mihalas 1984) and updated during each time-step. The remaining variables in these equations represent the radius (r), the gas density (ρ), gas velocity (u), electron and ion gas pressures ($P_{e,i}$), electron and ion gas energies per unit mass ($e_{e,i}$), electron temperature (T_e), radiation flux (F_r) and the artificial viscosity (P_Q , see paper I). We neglect electron viscosity because it is typically smaller than the ion viscosity by a factor $(m_e/m_i)^{1/2}$.

The radiation hydrodynamics equation set (eqs. 1- 6) is supplemented with the adaptive grid equation (Gehmeyr and Mihalas 1994, Dorfi and Drury 1987). This equation distributes grid points so that discontinuities in the flow are resolved. In this work we found the best grid performance when we resolve the mass and the gas density.

The full set of equations is written in finite volume form using the adaptive mesh transport theorem (Winkler, Norman and Mihalas 1984) and then cast into finite difference form on a staggered grid (Gehmeyr and Mihalas 1994). The difference equations are linearized around the current solution and the solution at the next time step is calculated with a fully-implicit Newton-Raphson iteration.

2.1. The Model Problem

We consider a thin shell of gas extending from $R_i = 8.0 \times 10^6$ km to $R_o = 8.7 \times 10^6$ km. This problem is nearly plane parallel because $R_o - R_i \ll R_o$. Initially, the gas is at rest with constant density ($\rho_o = 7.78 \times 10^{-10}$ g/cm³) and a shallow temperature profile

$$T(r) = 10 + 75 \frac{r - R_i}{R_o - R_i} \text{K} \quad (7)$$

The sound speed in the gas is $c_s \lesssim 1$ km/sec. The gas has a constant absorptive opacity $\rho\kappa = 3.115 \times 10^{-10}$ cm⁻¹. These parameters are chosen to correspond to optically thick gas accreting onto a neutron star. Initially, the gas and radiation are in equilibrium and there is no net flux of radiation.

At time $t = 0$ a piston at R_i starts outward at a constant velocity, $u_p > c_s$, and a shock forms ahead of the piston. The shock propagates outward at a velocity

$$D = u_p / (1 - \eta_+) \quad (8)$$

where $\eta_+ = \rho_o / \rho_+$ is the shock compression ratio and ρ_+ is the gas density behind the shock. Note that $\eta_+ \gtrsim \eta_1$, where η_1 is the final compression ratio, because some additional compression can occur as the shocked gas cools from T_+ to T_1 . After a short time, $t \ll (R_o - R_i) / D$, the shock reaches a quasi-stationary state in which the structure of the shock front is independent of time when viewed in a frame moving at a velocity D , *i.e.*, with the shock front. We refer to the shock as quasi-stationary because as it propagates to larger distances geometric dilution of the spherical flow will cause an intrinsic time-dependence. In addition, the flow appears to fluctuate slightly near the piston. These fluctuations have no effect on the structure of the shock.

In this paper we assume that both the electron-ion energy exchange coefficient and the electron conduction coefficient are constant. In this case,

$$\Lambda_{ei} = \tau_{ei}^{-1} \quad (9)$$

is the inverse of the time-scale for electron-ion energy exchange. The electron conduction coefficient is

$$\kappa_{ec} = \frac{k_B}{m_p} l_e \bar{v}_e \quad (10)$$

where l_e is the electron mean free path and \bar{v}_e is the electron thermal velocity. The characteristic length scale for electron-ion energy exchange is $l_{ei} \sim \tau_{ei} D$ and that for electron conduction is $l_{ec} \sim \kappa_{ec} / D$. We neglect ion conduction and electron viscosity because they are comparatively small (Zel'dovich and Raizer 1967).

3. Results

Zel'dovich and Raizer (1967) defined two classes of shock wave structure for a single temperature fluid: subcritical and supercritical. Absorption of radiation from the shocked gas raises the temperature of the upstream material. A shock is called subcritical when the temperature of the preheated gas is smaller than the final downstream temperature. When the shock wave is stronger, preheating can raise the temperature of the upstream gas to be equal to, but never larger than, the final gas temperature (Zel'dovich and Raizer 1967).

Extending the classification scheme of Zel’dovich and Raizer (1967), we identify four types of shock front: subcritical, supercritical, electron subcritical and electron supercritical. When l_{ei} is small compared to the length scales for gradients in the flow variables, including the radiation mean free path, the electron and ion temperatures are nearly equal at all points in the flow. We classify these shocks using the standard notation because the temperature structure of these shocks is the same as the corresponding one-temperature shock wave.

The ion and electron temperatures decouple when l_{ei} is larger than the length scales for other gradients in the flow variables. For example, the length scale for radiative energy exchange in our model problem is $l_r = 1/\rho\kappa = 3.2 \times 10^9$ cm. In this case, preheating primarily affects the electron gas because there is not sufficient time for energy to be transferred from the electron gas to the ions. The shock structure is electron subcritical if the temperature of the preheated electron gas is smaller than the final temperature of the electron gas. When the temperature of the preheated electron gas becomes equal to the final electron temperature, the shock is electron supercritical. In both cases, the $T_i \lesssim T_e$ upstream from the shock and $T_i \gtrsim T_e$ downstream.

The kinetic energy of the inflowing gas is converted to thermal energy in the ion gas at the shock discontinuity. The temperature of the shocked ion gas is $T_i \sim m_i D^2/k$, where m_i is the mass of the ions. The hot ion gas cools by Coulomb collisions with the cold electrons. If l_{ei} is smaller than the shock standoff distance and all the kinetic energy of the infalling gas is converted into thermal energy, then the ion and electron temperatures equalize at the final value

$$T_1 \simeq \frac{1}{2} \frac{m_p}{k_B} \eta_1 (1 - \eta_1)^{-2} u_p^2 \simeq 27 u_{p,5}^2 \text{K}, \quad (11)$$

where $u_{p,5}$ is the piston speed in 10^5 cm/sec. The final temperature of the gas flowing through a supercritical shock is somewhat smaller than this value because the electron gas radiates a large part of the inflowing energy.

The ion temperature in the shocked gas remains larger than the electron temperature if l_{ei} is large. This has two consequences. First, the final ion temperature is larger than T_1 and the final electron temperature is smaller than T_1 . Second, the temperature of the preheated gas is lower because the temperature of the shocked electron gas is lower. This reduces the amount of energy which is radiated by the shocked gas. If l_{ei} is large enough (section 3.5.), the shock doesn’t become supercritical at any piston speed.

In the following sections, we present results of our simulations for four sets of the parameters l_{ei} and l_{ec} . They illustrate the effects of electron-ion energy exchange and electronic heat conduction on the structure of a radiating shock wave. In each case we plot the results for two piston speeds, 4 km/sec and 14 km/sec, which correspond to subcritical and supercritical shock strengths, respectively.

Figures 1 - 8 each contain at least two panels: one shows the electron (dashed line) and ion (solid line) temperatures as a function of optical depth from the shock front (τ) and the other shows the radiation (solid line) and electron conduction (dashed line) fluxes as a function of τ . In

Figs. 5 - 8 we also include a third panel containing a detail of the temperature structure in the shock front. The values of l_{ei} and l_{ec} for the models in this paper are listed in table 1.

3.1. $\Lambda_{ei} = 10^{-4} \text{ sec}^{-1}$, $l_e \bar{v}_e = 10^{11} \text{ cm}^2 / \text{sec}$

The temperature and radiation profiles of the subcritical shock wave are shown in Figs. 1a,b. This is an example of the structure of an electron subcritical shock wave. The electron-ion energy exchange length is on the order of 1% of the total width of the gas shell (see table 1). This is nearly the same as the radiation mean free path which implies that electron-ion energy exchange occurs as rapidly as electron radiative cooling. We find that $T_i \gg T_e$ immediately behind the shock but the temperatures equalize $5 \times 10^{10} \text{ cm}$ behind the shock (Fig. 1a). Although this distance is about a factor of ten larger than l_{ei} , the length scale over which the cooling occurs is comparable to l_{ei} . Electron conduction and radiative heating raise the preshock electron temperature by a small amount.

The radiation flux in this case is small and has a roughly exponential profile (Fig. 1b). The radiation energy density is much larger than the equilibrium value of $e_{r,eq} = a_r T_e^4$, as expected for a subcritical shock (Sincell, *et al.* 1997). Electron conduction smooths the gradient in the electron temperature profile, so the sharp peak in the radiation flux profile of the one-temperature gas (Sincell, *et al.* 1997) is rounded off.

The electron conduction flux at the shock front

$$F_c = \rho \kappa_{ec} \frac{\partial T_e}{\partial r} \quad (12)$$

is many orders of magnitude larger than the radiation flux because of the large gradient in T_e at the shock front. However, l_{ec} is much smaller than a radiation mean free path so electron conduction has a very small effect upon the temperature profile.

The shock wave becomes electron supercritical when $u_p \gtrsim 10 \text{ km/sec}$ (Fig. 2a). The increased piston speed reduces l_{ei} so that it is much smaller than a radiation mean free path and the electron and ion gases are nearly decoupled. The ions upstream from the shock are preheated by the hot electron gas, but $T_e \gtrsim T_i$ upstream from the shock because of the large value of l_{ei} . Similarly, the ion gas is cooled by Coulomb collisions with the colder electron gas but $T_i \gtrsim T_e$ downstream from the shock.

The electron gas and the radiation field are in equilibrium from the shock discontinuity to an optical depth of $\tau \sim 3$. In this region the gas temperature falls roughly as (see Sincell, *et al.* 1997)

$$T_e \propto \left(1 + \frac{3\sqrt{3}}{4} |\tau - \tau_c| \right)^{1/3} \quad (13)$$

where τ_c is the optical depth where the electron gas and the radiation field fall out of equilibrium.

The ratio of the peak electron temperature to the post shock temperature is nearly 1.5, as expected for a supercritical shock wave (Sincell, *et al.* 1997). Electronic heat conduction does not reduce the amplitude of the spike because l_{ec} is much smaller than the length scale of the temperature spike. Note that in Fig. 2ab the T_e and F_c profiles have been offset from the T_i and F_r profiles so that the spikes at the shock radius can be seen.

The radiation flux profile (Fig. 2b) is very similar to that of a supercritical wave in the one temperature fluid, again reflecting the weak coupling of the electron and ion fluids and the small conduction length scale. The peak value of F_c is again much larger than the peak of the radiation flux. Electron conduction is effective in keeping T_e approximately constant near the piston, whereas T_i drops rapidly.

3.2. $\Lambda_{ei} = 10^{-4} \text{ sec}^{-1}$, $l_e \bar{v}_e = 10^{15} \text{ cm}^2 / \text{sec}$

Another example of an electron subcritical wave is displayed in Fig. 3. In this case, we find that $l_{ec} \simeq l_{ei} \simeq 10^9 \text{ cm}$ (table 1). The conduction length is now comparable to the radiation mean free path, so electron conduction is effective in preheating the upstream electron gas. The temperature profile of the preheated electrons falls exponentially on a scale l_{ec} . Conduction also removes the discontinuity in T_e at the shock radius (Fig. 3a).

Both the conduction and radiation fluxes drop exponentially with distance from the shock (Fig. 3b). The length scale for the F_c profile is l_{ec} so the profile is broader, and the peak flux is much lower, than in model 1. The F_r profile is largely unchanged when the conductivity is increased. The length scale for F_r is set by the (constant) opacity and the final value of T_e behind the shock is very close to the value in model 1. Conduction is only effective in regions where the T_e gradient is large, so it is not surprising that it has little effect upon the temperature behind the shock.

The shock wave becomes electron supercritical when $u_p = 14 \text{ km/sec}$. The F_r and T_e profiles for this model are very similar to those in model 2 (Figs. 4ab). The only effect that the increase in the conductivity has is to reduce the T_e spike to a small blip at the shock radius. The width of this blip is on the order of l_{ec} . Although radiation heats the electron gas to $T_e \gg T_i$, the electron-ion exchange length is large and a discontinuity in T_i remains at the shock radius. The conduction flux is also smaller in this case.

3.3. $\Lambda_{ei} = 10^{-2} \text{ sec}^{-1}$, $l_e \bar{v}_e = 10^{11} \text{ cm}^2 / \text{sec}$

The length scale for the electron-ion energy exchange is reduced by two orders of magnitude in these models. We find that $T_e = T_i$ on virtually all length scales and when plotted as a function of radius they are nearly indistinguishable (Fig. 5a). However, if we plot T_e and T_i as a function of grid point (Fig. 5b) we can see that $T_i > T_e$ in the shock front. The two temperatures rapidly equilibrate after the shock and the width of the spike in T_i at the shock front is roughly l_{ei} . This demonstrates the unique power of the adaptive grid to resolve physical quantities on multiple length scales.

The shock wave is subcritical when $u_p = 4$ km/sec and F_r has the familiar exponential profile. The F_c profile is strongly peaked at the shock radius but it also has a broad peak behind the shock. This is caused by the strong electron-ion coupling which forces T_e to follow T_i and introduces curvature into the T_e profile.

The structure of the two-temperature shock wave in the supercritical case (Fig. 6abc) is almost identical to a supercritical shock in the one-temperature approximation (paper I). This is not surprising because the small length scale for energy exchange implies that the two fluids are completely coupled.

The only departures from the one-temperature approximation occur in the shock front, where $T_e \lesssim T_i$. The reduction in the electron temperature reduces the flux from the supercritical two-temperature shock by a few percent relative to the one-temperature fluid (Sincell, *et al.* 1997). The electron conduction flux has a very large peak, caused by the spike in T_e , but it has a negligible effect upon the temperature distribution because l_{ec} is small.

3.4. $\Lambda_{ei} = 10^{-2} \text{ sec}^{-1}$, $l_e \bar{v}_e = 10^{15} \text{ cm}^2 / \text{sec}$

Increasing the electron conductivity in the strongly coupled fluid does not have any pronounced effects upon the structure of the shock wave (Figs. 7abc and 8abc). The enhanced conduction makes the post shock gas in the subcritical flow nearly isothermal and there is a small amount of preheating of the electron gas (Fig. 7b). We also see that the F_c profile is slightly broadened ahead of the shock.

Electron conduction reduces the peak of T_e in the supercritical case. The radiation flux is therefore smaller in this case.

3.5. Critical Energy Exchange Rate

We find that no supercritical shock develops at any speed when $\tau_{ei} \gtrsim \tau_{ei,c} = 2 \times 10^5$ seconds because the low rate of electron-ion energy exchange reduces the gradient in the electron energy

density, limiting the radiative flux. The radiation flux from the shocked gas is given approximately by the diffusion equation

$$F_r \simeq \frac{16\sigma T^3}{\rho\kappa} \frac{dT}{dr} \quad (14)$$

because the gas is optically thick. The length scale for heating the electron gas by electron-ion energy exchange is l_{ei} so $F_r \lesssim F_c = \sigma T_c^4$ when

$$\tau_{ei} \gtrsim \tau_{ei,c} = \frac{16}{3} \frac{T}{T_c} \frac{1}{\rho\kappa D} \quad (15)$$

where T_c and F_c are the critical temperature and radiation flux (see Sincell, *et al.* (1997)). Assuming that $T = T_c$ and $D = 10$ km/sec, we find $\tau_{ei,c} = 2 \times 10^5$ seconds.

4. Conclusions

We have solved the time-dependent spherically-symmetric equations of radiation hydrodynamics on an adaptive grid for a fully ionized gas. We treat the gas as a two-temperature fluid and neglect recombination. The time scale for electron-ion energy exchange, τ_{ei} , and the electron conduction coefficient, κ_{ec} , are assumed to be constant free parameters of the problem. The gas opacity is constant and purely absorptive.

In this paper, the shock wave is created by moving a supersonic piston into a constant density shell of cold, but fully ionized, gas. The shock propagates into the gas at a speed $D = u_p/(1 - \eta_+)$, where η_+ is the compression ratio just downstream of the shock front, and we find that the structure of the shock becomes steady in the shock frame after a time short compared to the flow time. The temperature of the shocked gas is approximately $T_1 \simeq 27u_{p,5}^2$ K, where $u_{p,5}$ is the piston speed in 10^5 cm/sec.

Shocks in a two-temperature gas can be grouped into four general categories depending on the piston speed and the length scale for electron-ion energy exchange, $l_{ei} = \tau_{ei}D$.

For our model problem, the shock wave is electron subcritical when $l_{ei} \gtrsim 10^4$ km and $u_p \lesssim 9$ km/sec. We find that $T_i > T_e$ behind the electron subcritical shock because of the slow transfer of energy from ions to the electrons. There is no preheating of either electrons or ions. The shock becomes electron supercritical when $u_p \gtrsim 10$ km/sec. In this case, preheating of the electron gas raises the pre-shock T_e to be equal to the post shock value. However, the slow transfer of energy from the electrons to the ions prevents preheating of the ion gas. Thus, $T_i > T_e$ behind the shock and $T_i < T_e$ ahead of the shock.

We find that an electron supercritical shock cannot form when $\tau_{ei} \gtrsim 2 \times 10^5$ sec. The transfer of energy is so slow that T_e remains too low to preheat the electron gas.

The electron and ion temperatures are nearly equal at all points in the flow when $l_{ei} \lesssim 10^3$ km because the electron-ion energy exchange is very efficient. For $u_p \lesssim 9$ km/sec, the shock wave is subcritical and for larger u_p it becomes supercritical. The structure of the shock wave is nearly identical to that of a single temperature fluid, as described in paper I.

Electronic conduction smooths the T_e profile on lengths $l_{ec} \sim \kappa_{ec}/D$. The radiation flux is roughly proportional to the gradient in T_e , so larger conduction coefficients tend to reduce the radiation flux.

REFERENCES

- Burger HL, Katz JI (1983) The Eddington limit and supercritical accretion II: Time-dependent calculations. *Astroph. J.* 265:393-401
- Dorfi EA, Drury LO'C, (1987) Simple adaptive grids for 1D initial value problems. *Physica D.* 69:175
- Gehmeyr M, Mihalas D, (1994) Adaptive grid radiation hydrodynamics with TITAN. *Physica D* 72:320-???
- Mihalas D, Mihalas BW (1984) *Foundations of Radiation Hydrodynamics*, Oxford University Press, Oxford
- Tscharnutter WM, Winkler KH (1979) A method for computing self gravitating gas flows with radiation. *Comput. Phys. Commun.* 18:171
- Winkler KH, Norman ML, Mihalas D (1984) Adaptive mesh radiation hydrodynamics-I. The radiation transport equation in a completely adaptive coordinate system. *J.Q.S.R.T.* 31:473-478
- Klein RI, Stockman HS, Chevalier RA (1983) Supercritical time-dependent accretion onto compact objects I: Neutron stars. *Ap.J.* 237:912-930
- Shafranov VD (1957), The structure of shock waves in a plasma. *Sov. Physics JETP* 5:1183-1188
- Sincell MW, Gehmeyr M, Mihalas D (1997), The Quasi-stationary Structure of Radiating Shock Waves I: The One-temperature Fluid, to appear in *Shock Waves*
- Zel'dovich YB, Raizer YP (1967) *Physics of Shock Waves and High Temperature Hydrodynamic Phenomena*, Academic Press, New York

5. Figure and Table Captions

Table 1. Parameters and length scales for the models presented in this paper. Symbols are defined in the text.

Figure 1. The electron (dashed) and ion (solid) temperatures for model 1 are plotted as a function of optical depth in (a). The corresponding radiation (solid) and electron conduction (dashed) fluxes are in (b). The peak of the electron conduction flux is much larger than the scale of this plot.

Figure 2. Model 2. Note that the electron temperature and the conduction flux profiles are displaced by a small amount to show the spike at the shock radius.

Figure 3. Model 3

Figure 4. Model 4. The electron temperature has been displaced by a small amount to show the temperature spike at the shock radius.

Figure 5. The electron and ion temperatures for model 5 are plotted as a function of optical depth in (a) and as a function of grid index in (b). The corresponding radiation and electron conduction fluxes are in (c). The peak electron conduction flux is larger than the scale of this plot.

Figure 6. Model 6. The peak of the electron conduction flux is larger than the scale of this plot.

Figure 7. Model 7

Figure 8. Model 8

Model	$\Lambda_{ei}(\text{sec}^{-1})$	$(l\bar{v})_c(\text{cm}^2/\text{sec})$	$u_p(\text{km}/\text{sec})$	l_{ei} cm	l_{ec} cm
1	10^{-4}	10^{11}	4	4×10^9	3×10^5
2			14	1×10^{10}	9×10^4
3	10^{-4}	10^{15}	4	4×10^9	3×10^9
4			14	1×10^{10}	9×10^8
5	10^{-2}	10^{11}	4	4×10^7	3×10^5
6			14	1×10^8	9×10^4
7	10^{-2}	10^{15}	4	4×10^7	3×10^9
8			14	1×10^8	9×10^8

Table 1:

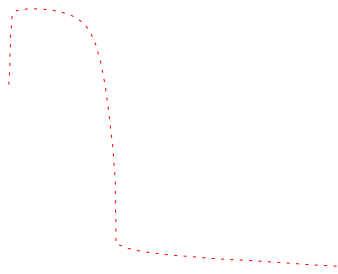


Fig. 1.—

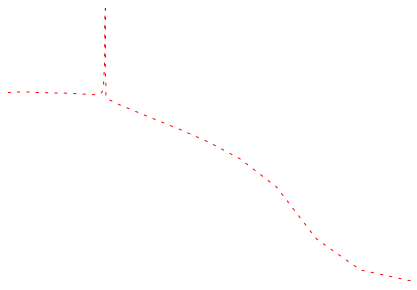


Fig. 2.—

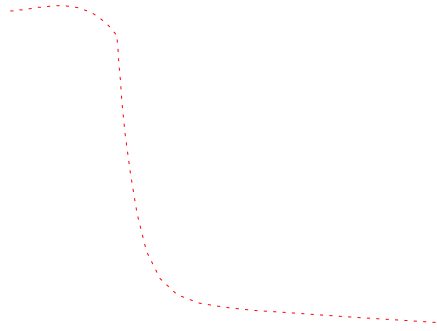


Fig. 3.—

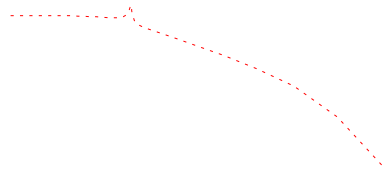


Fig. 4.—



Fig. 5.—

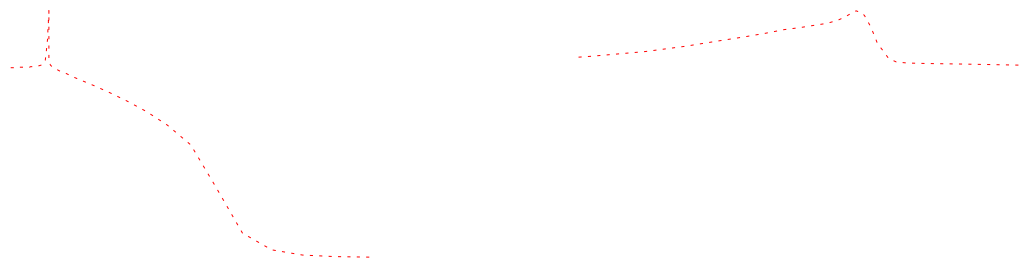


Fig. 6.—



Fig. 7.—



Fig. 8.—